POLITECNICO DI TORINO
Repository ISTITUZIONALE

On the Static Performance of Concave Aerostatic Pads

(Article begins on next page)

25 April 2024

On the Static Performance of Concave Aerostatic Pads

Federico Colombo[1], Luigi Lentini[1*], Terenziano Raparelli[1], Vladimir Viktorov[1],

Andrea Trivella[1]

[1] Politecnico di Torino, Turin (TO) 10129, Italy
* luigi.lentini@polito.it

Abstract. Numerical models have been largely utilized as a valuable tool to investigate the performance of aerostatic pads. These models make it possible to evaluate the effect of different parameters, e.g., supply pressure, orifices diameter and locations. This paper presents a numerical study to investigate to what extent the use of concave surfaces can modify the static performance of aerostatic pads. The study consists in comparing the performance of flat and concave pads in the presence of different supply pressures and maximum depths of concavity.

Keywords: concave profile, gas bearing, aerostatic pads, numerical model.

1   Introduction

Aerostatic bearings are widely used in many applications where their high accuracy and almost zero friction are of relevant importance. Metrology, ultra-precision machining and semi-conductor production equipment are some examples of these applications [1].

However, aerostatic bearings are characterized by low relative stiffness and poor damping [2]. Because of the current demand to have more performant bearings, different technical solutions have been proposed. Among the possible solutions, one of the most frequently adopted to achieve performance enhancement is designing feeding systems of different types, e.g., simple and pocketed orifices, compound restrictors, micro holes and porous surfaces. Lumped and distributed models represent a valuable aid to perform preliminary design and assessment of the bearings performance. Because of their low computational cost, lumped parameters models are usually employed to perform stability analysis and simulate the performance of aerostatic bearings exploiting passive and active compensation methods [3]. Blondeel et al. [4] proposed a feedback loop model to carry out the stability analysis of an aerostatic pad with a central pocketed orifice. In this kind of lumped models [5–9], the governing equations of the pad are linearized and used in combination with stability analysis methods. Ghodsiyeh et al. [10] used a lumped parameter model to design a passively compensated pad with an embedded diaphragm valve. Colombo et. al [11, 12] proposed an identification method to estimate the stiffness and damping of the air film of aerostatic pads and then used this method to simulate the performance of an actively compensated bearing exploiting the support compensation method [13, 14]. Conversely, distributed parameters models

are usually implemented through finite difference (FD) or finite element (FE) methods to obtain more accurate bearing characterizations. Colombo et al. [15] implemented a FD model based on the modified Reynolds equation (isothermal condition) to study the behavior of a rectangular pad with multiple orifices. The influence of the supply pressure, orifice location and size was investigated both in static and dynamic conditions. In the presence of symmetrical boundary and loading conditions, the complexity of the model can be significantly reduced by the use of polar coordinates. This can be the case of circular pad. Charki et al. [16] developed different finite element models to compare the performance of circular aerostatic pads with simple orifices, compound restrictors and porous surfaces. Additionally, distributed models make it possible to study the performance of bearings with non-flat surfaces. The use of this non-flat surfaces is a frequently used solution that was introduced for different reasons, e.g., avoiding adhesion and compensating for pad deflections.

This paper presents a numerical model used to investigated to what extent the planarity of pad surfaces can affect their static performance. The performance of aerostatic pads with multiple inherent orifices is compared in the presence of a flat and semi-ellipsoidal concave surfaces. The results of these comparisons show the possibility to study pads with concave surfaces as equivalent flat pads.

2 The model of the pad

The bearings under investigations are aerostatic pads with sizes of 75x50 mm^2 and thicknesses equal to 13 mm. These pads have flat or concave surfaces. The concave pads have of maximum depths of concavity of 1, 3 and 5 [μm]. Figure 1 shows a scheme of the active surface of the pads. The pads present eight supply holes with a diameter of 0.2 mm which are distributed on a supply rectangle of size 55x30 mm^2.
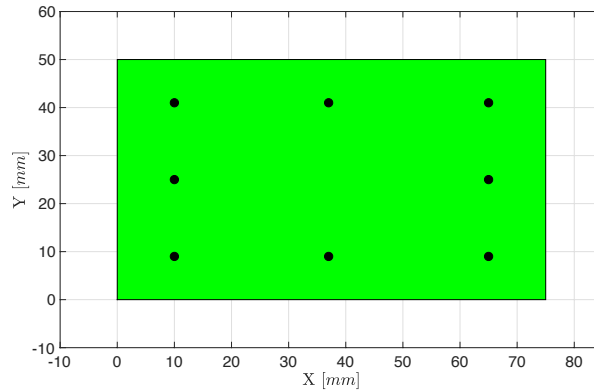

Fig. 1. Scheme of the active surface of the pad.

The bearing surface was discretized through FD method and Reynolds' equation (see Equation1) is used to compute its consumption and air gap pressure distribution.

$$\frac{\partial}{\partial x}\left(\rho \frac{\partial p}{\partial x}\frac{h^3}{12\mu}\right) + \frac{\partial}{\partial y}\left(\rho \frac{\partial p}{\partial y}\frac{h^3}{12\mu}\right) = \frac{\partial(\rho h)}{\partial t} \tag{1}$$

where h is the air gap height, p, μ and ρ are the air pressure, viscosity and density respectively. The adopted boundary condition to solve the problem are the inflow through the supply holes and the ambient pressure at the pad edges. The inflow through the supply holes is computed as:

$$G_{in} = c_d \frac{\pi d_s^2}{4}\frac{0.6855}{\sqrt{RT}}p_s\sqrt{1 - \Phi^2} \tag{2}$$

where, d_s and p_s are the hole diameter and the supply pressure. c_d is a discharge coefficient obtained through a semi-empirical formula [17]:

$$c_d = 0.85\left(1 - e^{-8.2\frac{h}{d_s}}\right)(1 - 0.3e^{-0.001Re}) \tag{3}$$

where Re is the Reynolds' number computed at the outlet of the considered supply hole:

$$Re = \frac{4G}{\pi\mu d_s} \tag{4}$$

Φ takes into account the pressure drop between the upstream (p_s) and downstream (p_c) pressures of supply holes:

$$\Phi = \frac{\frac{p_c}{p_s} - 0.528}{1 - 0.528} \tag{5}$$

The pressure in each element of the mesh are computing solving the non-linear algebraic system obtained by the discretization of Reynolds' equation (1). In correspondence of the supply holes the continuity equation is imposed in the discretized volume:

$$G_{in} - G_{out} = \dot{m} \tag{6}$$

where G_{out} is the mass air flow outflowing from the volume. The load capacity F of the bearing is computed by integrating the pressure distribution:

$$F = \int (p - p_a)\, dA \tag{7}$$

For reasons of simplicity, Euler's explicit method was employed to find the steady state solution. Figure 2 shows a flow chart of the employed computational algorithm. The solutions are obtained by iterative steps through pseudo-unsteady method [18].
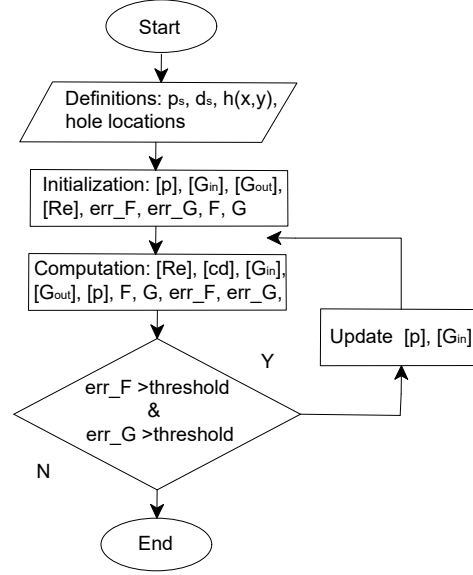
Fig. 2. Flow chart of the computational procedure

The first step of the procedure consists in defining the input parameters (supply pressure p_s, orifice diameter d_s, their locations, the air gap function $h(x, y)$). Secondly, inflow G_{in}, outflow G_{out}, air gap pressure p, load capacity F and air consumption G are initialized, along with the convergence errors:

$$err_F = \frac{(F_{iter+1} - F_{iter})}{F_{iter+1}} \neq 0 \tag{8}$$

and

$$err_G = \frac{(G_{iter+1} - G_{iter})}{G_{iter+1}} \neq 0 \tag{9}$$

The iterations continue by calculating in the order Re, G_{in}, G_{out}, p, F and G till the convergence errors become lower than the defined thresholds.

3   Methodology

Different numerical simulations were carried out to investigate the difference in performance between flat and concave aerostatic pads. Figure 2a shows the surface of the simulated concave pad. Here, to facilitate the visualization of the concave surface, the scale of the Z axis is enlarged. Figure 2b illustrates a sketch of the concave profile of the pad.
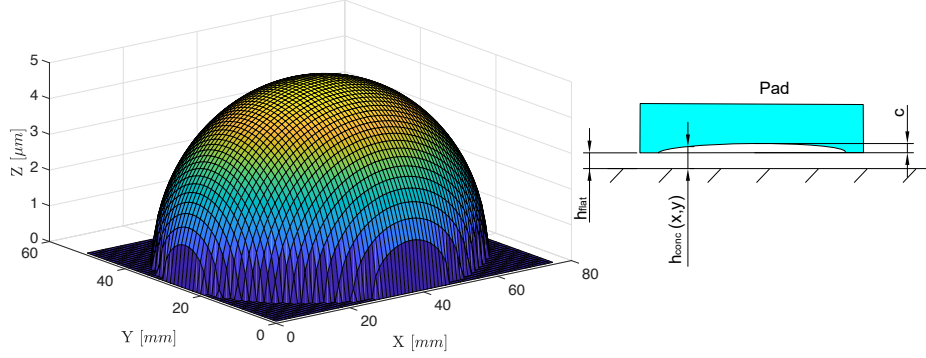
Fig. 3a. Semi-ellipsoidal surface of concave pads (c= 5 μm) **Fig 3b.** Profile of concave pads

Close to their edges the surfaces of concave pads are flat, whereas the inner regions are described by a semi-ellipsoidal function. This kind of surfaces was chosen to simulate a profile similar to those obtained through spherical milling. The mathematical expression of the concave gap is the following:

$$h_{concave} = h_{flat} + c \sqrt{1 - \left(\frac{x}{x_0}\right)^2 - \left(\frac{y}{y_0}\right)^2} \tag{7}$$

where, c is the maximum depth of the concave profile and h_{flat} is the air gap at the edges of the pad. Only positive values of $1 - (x/x_0)^2 - (y/y_0)^2$ were considered. The analysis was performed considering relative supply pressures (p_s) equal to 3, 4 and 5 bar and different depths of the concave profiles c= 1, 3 and 5 μm. The comparison of the performance of flat and concave pads was carried out taking into account their load capacity, air consumption and stiffness.

4   Results

Figures 4 to 6 show the static curves regarding the load capacity, air consumption and stiffness of the investigated flat and concave pads. These features are expressed as a function of the minimum air gap height of pads h_{flat} (see Figure 3b) in the presence of relative supply pressures equal to 3, 4 and 5 bar and different concavity depths c. As it can be seen in Figure 4, the load capacity of each pad increases with the supply pressure and it is possible to distinguish three different regions depending on the air gap height. The first region is located at air gaps smaller than 7-8 μm. Here, the load capacity of concave pads is always higher than those of flat bearings for each value of concavity. It is also worth noting that in this region, the curves of flat pads exhibit a saturation of their load capacities, whereas concave pads do not. Between air gaps of 7 and 8 μm flat concave pads exhibit similar load capacities. Conversely, at air gaps higher than 8 μm, the load capacity of the flat pads is always higher compared to that of their concave

counterparts. It appears that the load capacity decreases as the depth of concavity c increases.
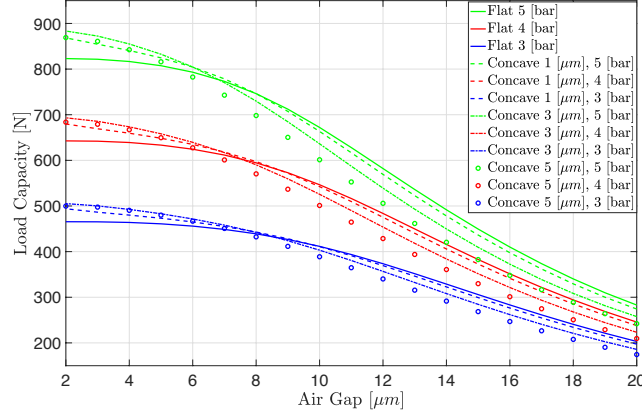

Fig. 4. Load Capacity vs minimum air gap height

Figure 5 compares the air consumption curves of the simulated pads. As expected, the air consumption increases as the supply pressure and the concavity depth increases.
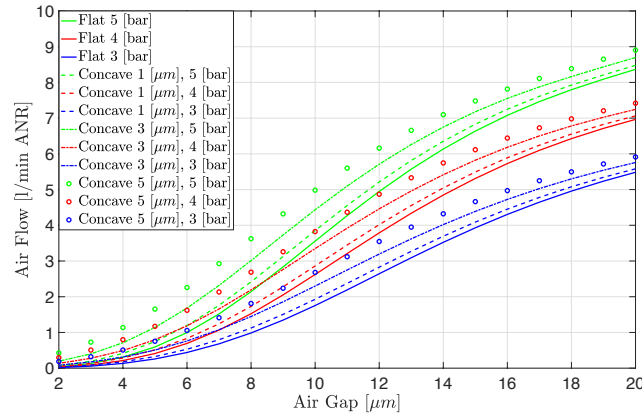

Fig. 5. Air consumption vs minimum air gap height

Figure 6 shows the static stiffness curves of the simulated pads. The stiffness of each pad increases with their supply pressure. Moreover, it is clear that concave pads exhibit stiffnesses that are higher than their flat counterparts up to about 5%. Secondly, the air gaps corresponding to the maximum stiffness of concave pads reduces as the concavity increases. Eventually, moving towards zero air gap condition, concave pads exhibit almost constant stiffnesses whereas, the stiffness of flat pads gradually reduces to zero.
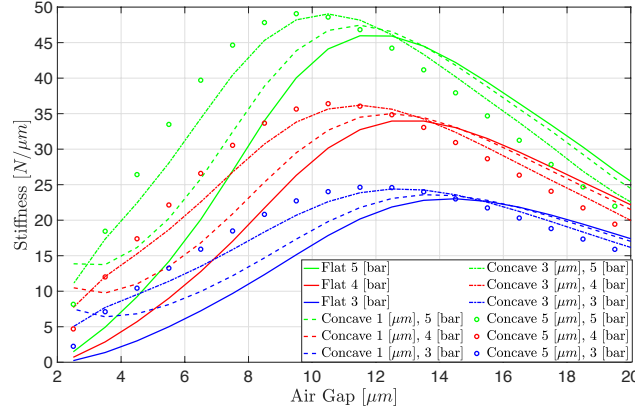
Fig. 6. Stiffness vs minimum air gap height

The analysis of the shift of the load curves in the third region allows the following relationships to be found:

Maximum depth of concavity c [μm]	Relationship ($h_{c,eqv}$ h_{flat}) [μm]
1	$h^*_{c1} = h_{flat} + 0.3$
3	$h^*_{c3} = h_{flat} + 1$
5	$h^*_{c5} = h_{flat} + 1.7$

where, h^*_{c1}, h^*_{c3} and h^*_{c5} are air gaps that make it possible to study a concave pad as an equivalent flat pad. Figure 7, 8 and 9 show the comparison between flat and concave pads considering these equivalent air gaps. As a confirm of this, Figure 7 shows that there is an almost perfect match between the air consumption curves (error less than 0.5 μm).
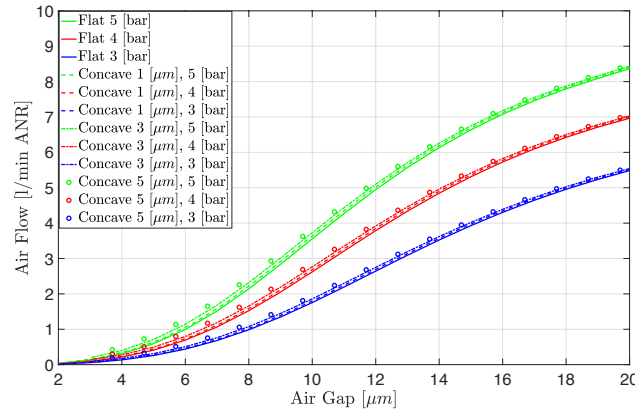

Fig. 7. Air consumption vs equivalent air gap height

Furthermore, similar results are evident in Figure 8. The load curves coincide at high

air gaps and then, because the presence of the semi-ellipsoidal recesses, the load capacity of concave pads gradually departs from those of the flat pads.
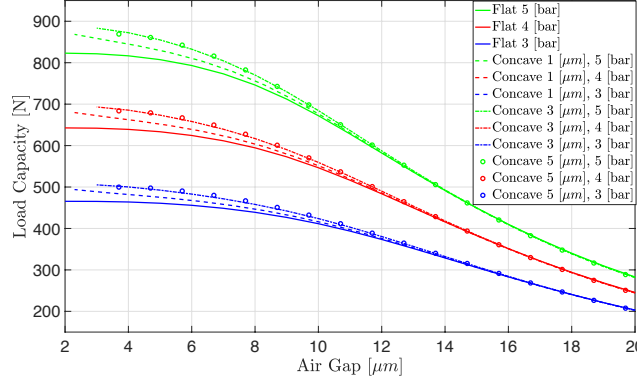

Fig. 8. Load capacity vs equivalent air gap height

The effect of the recesses of concave pads is more evident on the stiffness curves (see Figure 9). The stiffness of the equivalent concave pad is very similar to that of flat pads only at high air gap heights, where the volume of the recess can be considered negligible compared to that of the flat air gap. For smaller air gaps, the difference between the stiffness of equivalent concave and flat pads increases as the air gap height reduces. Eventually the stiffness of concave pads tends to constant values whereas that of flat pads tends to zero.
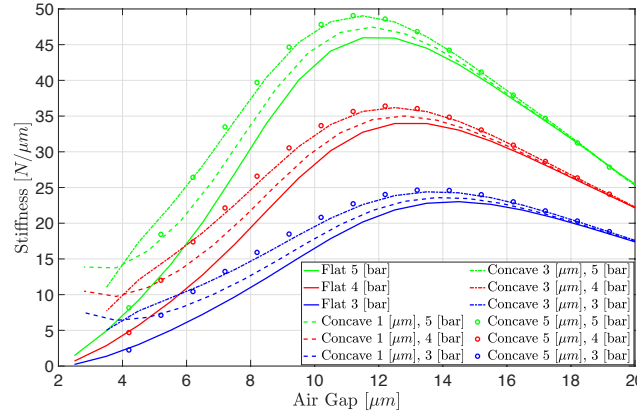

Fig. 9. Stiffness vs equivalent air gap height

5 Conclusions

This paper compares the performance of concave and flat aerostatic pads with multiple inherent orifices. The comparison was carried out through FD models of the two types

of pads. The obtained results show that, at the same minimum air gap height, concave pads exhibit always higher stiffness and air consumptions. Meanwhile, regarding load capacity, it is necessary to distinguish among three different regions. The first zone is at air gap heights lower than 7 μm, where concave pads exhibit higher load capacity than the flat pads. Conversely, in the third region the opposite trend occurs. Between these two regions there is a transitional zone where the two types of pads have similar load capacity. However, the most promising outcome of this investigation was that by considering a modified air gap height, the performance of a concave pad can be studied as that of an equivalent flat pad. This result is relevant because equivalent air gap heights could be exploited to extend the use of lumped models also in the case of non-flat pads, e.g., for concave [19] and grooved bearings [20].

6   References

1.   Lentini, L., Moradi, M., Colombo, F.: A Historical Review of Gas Lubrication: From Reynolds to Active Compensations. Tribology in Industry. 40, 165–182 (2018). doi:10.24874/ti.2018.40.02.01

2.   Al-Bender, F.: On the modelling of the dynamic characteristics of aerostatic bearing films: From stability analysis to active compensation. Precision Engineering. 33, 117–126 (2009). doi:http://dx.doi.org/10.1016/j.precisioneng.2008.06.003

3.   Raparelli, T., Viktorov, V., Colombo, F., Lentini, L.: Aerostatic thrust bearings active compensation: Critical review. Precision Engineering. 44, 1–12 (2016). doi:http://dx.doi.org/10.1016/j.precisioneng.2015.11.002

4.   Blondeel, E., Snoeys, R., Devrieze, L.: Dynamic Stability of Externally Pressurized Gas Bearings. Journal of Lubrication Technology. 102, 511–519 (1980)

5.   Richardson, H.H., Cambridge, M.: Static and dynamic characteristics of compensated gas bearings. Trans. of the ASME. 1503–1509 (1958)

6.   Roudebush, W.H.: An analysis of the effect of several parameters on the stability of an air lubricated hydrostatic thrust bearing. Technical note / National Advisory Committee for Aeronautics ; 4095, Washington (1957)

7.   Licht, L., Fuller, D.D., Sternlicht, B.: Self-excited vibrations of an air-lubricated thrust bearing. Trans. ASME. 80, 411–414 (1958)

8.   Colombo, F., Lentini, L., Raparelli, T., Trivella, A., Viktorov, V.: A Lumped Model for Grooved Aerostatic Pad. In: Advances in Service and Industrial Robotics. pp. 678–686. Springer International Publishing (2018)

9.   Colombo, F., Lentini, L., Raparelli, T., Trivella, A., Vladimir, V.: A nonlinear lumped parameter model of an externally pressurized rectangular grooved air pad bearing. In: Advances in Italian Mechanism Science. pp. 490–497. Springer (2018)

10.   Ghodsiyeh, D., Colombo, F., Raparelli, T., Trivella, A., Viktorov, V.: Diaphragm valve-controlled air thrust bearing. Tribology International. 109, 328–335 (2017)

11.   Colombo, F., Lentini, L., Raparelli, T., Viktorov, V.: Experimental Identification of an Aerostatic Thrust Bearing. In: Advances in Italian Mechanism Science. pp. 441–448. Springer (2017)

12.   Colombo, F., Lentini, L., Raparelli, T., Viktorov, V.: Actively compensated aerostatic

thrust bearing: design, modelling and experimental validation. Meccanica. 1–16 (2017). doi:10.1007/s11012-017-0689-y

13. Aoyama, H., Watanabe, I., Akutsu, K., Shimokohbe, A.: An Ultra Precision Straight Motion System (1st Report). Journal of the Japan Society for Precision Engineering. 54, 558–563 (1988). doi:10.2493/jjspe.54.558

14. Matsumoto, H., Yamaguchi, J., Aoyama, H., Shimokohbe, A.: An Ultra Precision Straight Motion System (2nd Report). Journal of the Japan Society for Precision Engineering. 54, 1945–1950 (1988). doi:10.2493/jjspe.54.1945

15. Colombo, F., Lentini, L., Raparelli, T., Trivella, A., Viktorov, V.: Dynamic Characterisation of Rectangular Aerostatic Pads with Multiple Inherent Orifices. Tribology Letters. 66, (2018). doi:10.1007/s11249-018-1087-x

16. Charki, A., Diop, K., Champmartin, S., Ambari, A.: Numerical simulation and experimental study of thrust air bearings with multiple orifices. International Journal of Mechanical Sciences. 72, 28–38 (2013). doi:10.1016/j.ijmecsci.2013.03.006

17. Belforte, G., Raparelli, T., Viktorov, V., Trivella, a.: Discharge coefficients of orifice-type restrictor for aerostatic bearings. Tribology International. 40, 512–521 (2007). doi:10.1016/j.triboint.2006.05.003

18. Peyret, R., Viviand, H.: Pseudo-Unsteady Methods for Inviscid or Viscous Flow Computation. In: Casci, C. and Bruno, C. (eds.) Recent Advances in the Aerospace Sciences: In Honor of Luigi Crocco on His Seventy-fifth Birthday. pp. 41–71. Springer US, Boston, MA (1985)

19. Holster, P.L., Jacobs, J.A.H.: Theoretical analysis and experimental verification on the static properties of externally pressurized air-bearing pads with load compensation. Tribology International. 20, 276–289 (1987). doi:http://dx.doi.org/10.1016/0301-679X(87)90028-4

20. Colombo, F., Lentini, L., Raparelli, T., Trivella, A., Viktorov, V.: Dynamic model of a grooved thrust bearing: Numerical model and experimental validation. Presented at the AIMETA 2017 - Proceedings of the 23rd Conference of the Italian Association of Theoretical and Applied Mechanics (2017)